(μ-1,2-Peroxo)diiron(III/III) Complex as a Precursor to the Diiron(III/IV) Intermediate X in the Assembly of the Iron-Radical Cofactor of Ribonucleotide Reductase from Mouse†

Danny Yun,‡ Ricardo García-Serres,‖ Brandon M. Chicalese,‡ Young H. An,‡ Boi Hanh Huynh,‖ and J. Martin Bollinger, Jr.*,‡,§

Department of Biochemistry and Molecular Biology and Department of Chemistry, The Pennsylvania State University, University Park, Pennsylvania 16802, and Department of Physics, Emory University, Atlanta, Georgia 30322

Received August 22, 2006; Revised Manuscript Received December 4, 2006

ABSTRACT: Stopped-flow absorption and freeze-quench electron paramagnetic resonance (EPR) and Mössbauer spectroscopies have been used to obtain evidence for the intermediacy of a (μ-1,2-peroxo)-diiron(III/III) complex on the pathway to the tyrosyl radical and (μ-oxo)diiron(III/III) cluster during assembly of the essential cofactor in the R2 subunit of ribonucleotide reductase from mouse. The complex accumulates to ~0.4 equiv in the first few milliseconds of the reaction and decays concomitantly with accumulation of the previously detected diiron(III/IV) cluster, **X**, which generates the tyrosyl radical and product (μ-oxo)diiron(III/III) cluster. Kinetic complexities in the reaction suggest the existence of an anti-cooperative interaction of the monomers of the R2 homodimer in Fe(II) binding and perhaps O_2 activation. The detection of the (μ-1,2-peroxo)diiron(III/III) complex, which has spectroscopic properties similar to those of complexes previously characterized in the reactions of soluble methane monooxygenase, stearoyl acyl carrier protein Δ^9 desaturase, and variants of *Escherichia coli* R2 with the iron ligand substitution, D84E, provides support for the hypothesis that the reactions of the diiron-carboxylate oxidases and oxygenases commence with the formation of this common intermediate.

The R2 subunits of the class I ribonucleotide reductases (hereafter, simply R2[1]) from *Escherichia coli*, *Saccharomyces cerevisiae*, and mammals such as *Mus musculus* and *Homo sapiens* are members of the diiron-carboxylate family of oxidase and oxygenase proteins (*1*−*3*). Members of this family use carboxylate-bridged diiron(II/II) clusters to activate dioxygen for difficult oxidation reactions (*2*, *4*). Other members include soluble methane monooxygenase (sMMO), toluene-4-monooxygenase, and stearoyl acyl carrier protein Δ^9-desaturase (*4*). R2 is unique among these proteins in activating O_2 for a *one-electron* oxidation outcome, the formation of a stable tyrosyl radical from an endogenous, buried tyrosine residue (*5*−*7*). Consistent with this unique outcome, the reaction intermediate responsible for the generation of the functionally essential tyrosyl radical and the adjacent (μ-oxo)diiron(III/III) cluster in the final step of the reaction is a diiron(III/IV) cluster, denoted **X**, that is more oxidized than the product cluster by a single electron (*8*−*11*). Currently, cluster **X** is the only oxidized diiron intermediate in the reaction of a wild-type R2 protein that has been trapped at a concentration sufficient for definitive characterization (*8*, *9*). In contrast, two distinct oxidized diiron intermediates, the (μ-1,2-peroxo)diiron(III/III) complex (**P** or $\mathbf{H_{peroxo}}$), and the methane-hydroxylating diiron(IV/IV) complex, **Q**, have been shown to accumulate in sequence during O_2 activation by sMMO (*12*, *13*). In accord with the hydroxylating (two-electron oxidation) function of sMMO, both **P** and **Q** are more oxidized than the final diiron(III/III) product cluster by two electrons. In the case of the R2 reaction, following the formation of the presumptive initial diiron(II/II)-O_2 adduct, denoted as $(Fe_2O_2)^{4+}$, the rapid transfer of a single electron from a near surface tryptophan residue (W48 in *E. coli* R2) to the $(Fe_2O_2)^{4+}$ complex leads to the generation of a readily reducible W cation radical and **X** (*14*). Due primarily to the presence of this apparatus to ensure the rapid shuttling of an electron into the reacting diiron center, the nature of the one or more $(Fe_2O_2)^{4+}$ complexes preceding **X** in the R2 reaction has not been definitively established.

To provide a unifying theme for the O_2-activation mechanisms employed by the various diiron-carboxylate oxidases and oxygenases, it was proposed that the reactions commence with the formation of a common (μ-1,2 peroxo)diiron(III/III) complex (*15*, *16*). The different decay products of this common peroxodiiron(III/III) complex observed in the different reactions (e.g., **X** in R2 and **Q** in sMMO) were suggested to reflect the effects of divergent protein control of the reaction pathway for the desired reaction outcome (*15*,

† This work was supported by grants from the National Institutes of Health (GM55365 to J.M.B. and GM47295 to B.H.H.).

* To whom correspondence should be addressed. Tel: (814) 863-5707. Fax: (814) 863-7024. E-mail: jmb21@psu.edu.

‡ Department of Biochemistry and Molecular Biology.

§ Department of Chemistry, The Pennsylvania State University.

‖ Emory University.

[1] Abreviations: R2, R2 subunit of ribonucleotide reductase; EPR, electron paramagnetic resonance; Fe(II)-complexed R2, apo R2 incubated with Fe(II); FQ, freeze-quench; k_{obs}, observed apparent first-order rate constant; Y177•, tyrosyl radical in mouse R2; Y122•, tyrosyl radical in *E. coli* R2.

10.1021/bi061717n CCC: $37.00
Published on Web 01/27/2007

16). In a previous investigation of the reaction of O_2 with Fe(II)-complexed wild-type R2 from *Escherichia coli*, some evidence for accumulation of a sMMO-**P**-like (μ-1,2-peroxo)-diiron(III/III) intermediate very early in the reaction was obtained (*17*). Unfortunately, the low level of accumulation made it impossible to establish that the complex is on the pathway to **X**. Studies on *E. coli* R2 variants provided additional evidence for such an intermediate. Stoichiometric accumulation of a **P**-like complex was observed in the reactions of O_2 with variants with the D84E ligand substitution (*16*, *18*−*21*), and the decay of this complex was shown to lead in some cases to Y122 radical formation (*18*−*22*). However, the formation of cluster **X** from the **P**-like peroxide complex was never demonstrated for these R2 variants. More recently, experiments that combined mutagenesis, the chemical rescue approach, kinetic methods, and spectroscopy were carried out specifically to reveal the identity of the precursor to **X** (*23*, *24*). These experiments established that the rapid electron-transfer step that produces the **X**-W48+• state could be disabled by the W48A substitution (*23*, *25*), thus allowing the immediate precursor to **X** to accumulate in the reaction. Furthermore, these experiments showed that the disabled electron-transfer step could be restored by the introduction of an indole compound (*23*), triggering a rapid decay of the accumulated precursor with the concomitant formation of **X** (*24*). The nature of the immediate precursor to **X** was then revealed by spectroscopically identifying the species that accumulate in the reaction of the R2-W48A/Y122F variant and convert rapidly to **X** upon introduction of the indole compound (*24*). The results suggested that the immediate precursor to **X** is a diiron(III/III) complex, most likely with a bound peroxide equivalent, but with spectroscopic properties distinct from those of **P**. Two possible relationships of this precursor to the mechanism of the wild-type R2 reaction were considered. First, it might be an intermediate in a reaction pathway that is distinct from that followed by the wild-type protein and is engaged specifically as a result of the amino acid substitutions. Second, it might be an intermediate that also forms in the wild-type R2 reaction pathway but is normally prevented from accumulating by the fast electron-transfer step. In the latter case, the normal pathway might or might not involve a **P**-like precursor to the detected complex (*24*). Similarly, the (μ-1,2 peroxo)-diiron(III/III) complex detected in the D84E-containing R2 variants (*16*, *18*−*21*) could be a precursor to **X** stabilized by the D84E ligand substitution or, alternatively, a complex that forms in place of the natural precursor as a result of the ligand substitution. Thus, the published studies have so far failed to resolve definitively whether a **P**-like complex is on the pathway to tyrosyl radical formation in R2. In this work, we provide kinetic and spectroscopic evidence indicating that such a complex is indeed a precursor to cluster **X** in the reaction of wild-type R2 from mouse.

MATERIALS AND METHODS

Materials. Culture media components (yeast extract and tryptone) were purchased from Marcor Development Corporation (Hackensack, NJ). Isopropyl β-D-thiogalactopyranoside (IPTG) was purchased from Biosynth International (Naperville, IL). Spectinomycin dihydrochloride, phenylmethylsulfonyl fluoride (PMSF), streptomycin sulfate, Trizma base (Tris), and 1,10-phenanthroline were purchased from Sigma (St. Louis, MO). Ampicillin was purchased from IBI (Shelton, CT). Glycerol, ammonium sulfate, and sodium chloride were purchased from EM Science (Gibbstown, NJ). Enzyme grade 4-(2-hydroxyethyl)-1-piperazineethanesulfonic acid (HEPES) was purchased from FisherBiotech (Pittsburgh, PA).

Expression and Purification of Apo R2. BL21(DE3) cells containing the pMR2 and pSJS1240 plasmids were grown as previously described (*26*). Apo R2 was expressed and purified as previously described (*26*). After purification, the protein was dialyzed against 2 L of 100 mM HEPES buffer (pH 7.6) containing 24% (w/w) glycerol.

Stopped-Flow and Freeze-Quench Experiments. The apparatus and procedures employed for the stopped-flow absorption and freeze-quench EPR (FQ EPR) and Mössbauer (FQ Mössbauer) experiments have been described (*26*−*28*). The general procedure involved the removal of O_2 from the apo R2 solution as previously described (*29*), the addition of Fe(II) to the O_2-free apo protein (3.5−4.0 mol Fe(II) per mol R2 dimer) in an anoxic chamber, the initiation of the reaction by the mixing of the Fe(II)-complexed R2 with an O_2-saturated buffer solution in the Applied Photophysics SX18MV stopped-flow or Update Instruments System 1000 freeze/chemical-quench apparatus, and either the acquisition of absorption spectra in real time (stopped-flow) or the termination of the reaction at a desired time by rapid freezing (freeze-quenching). Details of the reaction conditions for each experiment are given in the appropriate Figure legend. During the course of this study, it was found that both the reaction temperature and the concentration of glycerol have a significant impact on the kinetics of the (μ-1,2-peroxo)diiron-(III/III) intermediate. Thus, stopped-flow absorption measurements were carried out over a range of temperature (5−25 °C) and glycerol concentration (3−36% w/w) to ascertain the best conditions for the spectroscopic characterization of this elusive reaction intermediate. The results indicated that optimal accumulation of the (μ-1,2-peroxo)diiron(III/III) intermediate could be attained with 24% (w/w) glycerol at 10 °C. These conditions were then chosen for the FQ EPR and Mössbauer measurements. Because the intermediate accumulates to its maximum concentration very early in the reaction under these conditions, high flow velocities (2 mL/s) were used in the FQ experiments to reduce the quench time. The reaction times given in the text and Figure legends are the sum of the known transit time through the FQ reaction hose and the best estimate for the quench time, 5 ms.

EPR and Mössbauer Spectroscopy. The spectrometers have been described (*9*, *28*). The conditions used in spectral acquisition are given in the Figure legends.

RESULTS AND DISCUSSION

Spectroscopic Evidence for the Accumulation of a (μ-1,2-Peroxo)diiron(III/III) Complex Early in the Reaction of Fe(II)-Complexed R2 with O_2. Upon the mixing of Fe(II)-complexed R2 with O_2-saturated buffer at 10 °C, a broad absorption feature with maximum intensity (λ_{max}) near 700 nm develops in the first few milliseconds (Figure 1). The spectrum taken 3 ms after mixing (blue spectrum in the inset) is almost identical to that of the (μ-1,2-peroxo)diiron(III/III) species that accumulates in the reaction of the *E. coli*

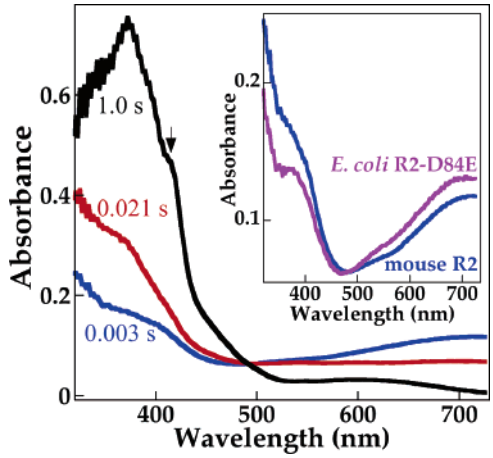

FIGURE 1: Absorption spectroscopic evidence for the accumulation of a (μ-1,2-peroxo)diiron(III/III) complex during O_2 activation by mouse R2. The spectra were acquired 3 ms (blue), 21 ms (red), and 1.0 s (black) after the mixing of an O_2-free solution at 10 °C containing 0.37 mM R2 and 1.5 mM Fe(II) in 100 mM Hepes (pH 7.6) and 24% glycerol with an equal volume of the same buffer saturated with O_2. The arrow indicates the 416-nm absorption arising from Y177•. The inset shows a comparison of the 3-ms spectrum (blue) to the kinetically resolved spectrum of the (μ-1,2 peroxo)diiron(III/III) intermediate in the reaction of *E. coli* apo R2-D84E with Fe(II) and O_2 (purple) (*18*).

R2-D84E variant (purple spectrum) (*18*). Subsequently, this 700-nm feature decays concomitantly with the development of the sharp absorption feature at 416 nm from the Y177• and the broader features at 365 and 600 nm from the (μ-oxo)diiron(III/III) cluster (*26*). The data suggest that a rapidly accumulating peroxodiiron(III/III) cluster is on the pathway to the product cofactor.

Further evidence for the early accumulation of a **P**-like (μ-1,2-peroxo)diiron(III/III) cluster was sought by FQ Mössbauer experiments. The 4.2-K Mössbauer spectrum of a sample freeze-quenched ~8 ms after mixing Fe(II)-complexed R2 with 2 equiv volumes of O_2-saturated buffer at 10 °C (spectrum B of Figure 2) comprises, in addition to the intense quadrupole doublet attributable to the reactant Fe(II)-complexed R2, a prominent absorption peak at ~1.5 mm/s (indicated by the arrow). A thorough analysis of the data indicates that this peak is the high-energy line of a quadrupole doublet (shown in blue) with parameters (δ = 0.63 ± 0.03 mm/s and ΔE_Q = 1.73 ± 0.05 mm/s) that are similar to those of compound **P** in sMMO (*12*, *13*) and the (μ-1,2-peroxo)diiron(III/III) complex in D84E variants of *E. coli* R2 (*18*, *20*).[2] The transient nature of this species is apparent from its reduced intensity in the spectra of samples quenched at later reaction times (compare spectra B and C in Figure 2). In the following sections, we show that the decay of this Mössbauer-detectable species coincides with the decay of the 700-nm feature observed in the stopped-flow absorption experiments. The association of the rapidly accumulating complex with these two spectroscopic features

[2] Although the low-energy line of the doublet arising from the peroxodiiron(III/III) intermediate overlaps with those of the doublets arising from the multiple Fe(II) species in Fe(II)-complexed R2, its position can be estimated with certainty by simultaneously analyzing the spectra of the early reaction time points, in which the accumulation of the intermediate is near maximal, together with the spectra of the samples of Fe(II)-complexed R2 prior to the O_2 reaction (e.g., spectrum A in Figure 2).

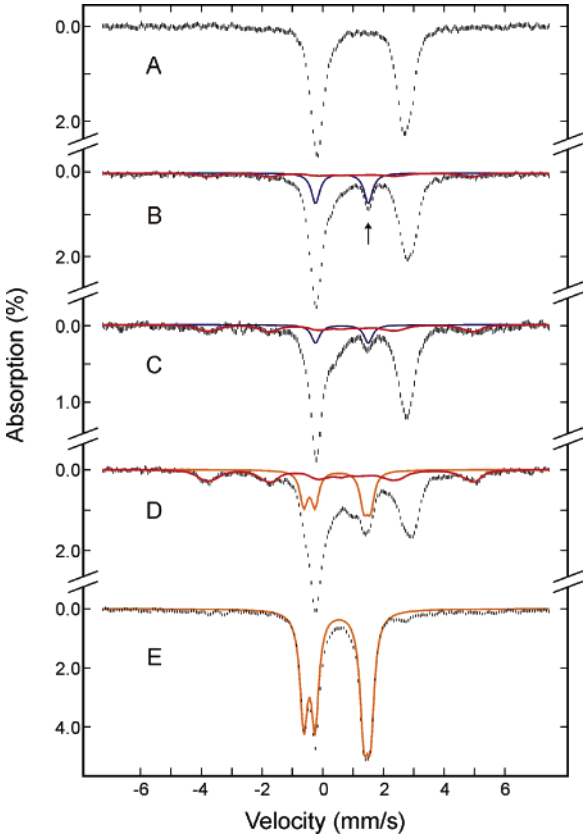

FIGURE 2: Mössbauer spectra of freeze-quenched samples from the reaction of Fe(II)-complexed R2 with excess O_2. An O_2-free solution of 1.2 mM R2 and 4.9 mM Fe(II) in 100 mM Hepes (pH 7.6) and 24% glycerol was mixed at 10 °C with 2 equiv volumes of the same buffer saturated with O_2. The samples were frozen (A) before mixing and (B) 0.008 s, (C) 0.026 s, (D) 0.15 s, (E) ~600 s after mixing. The colored solid lines plotted above the data are reference spectra of the (μ-1,2-peroxo)diiron(III/III) intermediate (blue; δ = 0.63 mm/s and ΔE_Q = 1.74 mm/s), cluster **X** (red; δ = 0.56, 0.26 mm/s, ΔE_Q = −0.9, −0.6 mm/s, $A_x/g_n\beta_n$ = −53.9, 20.0 T, $A_y/g_n\beta_n$ = −52.5, 26.8 T, $A_z/g_n\beta_n$ = −53.2, 26.8 T, respectively for the Fe(III) and Fe(IV) sites), and the (μ-oxo)diiron(III/III) cluster (orange; δ = 0.55, 0.47 mm/s, ΔE_Q = 1.61, 2.20 mm/s). They are plotted at the following intensities: blue, 0%, 15%, 9%, 0%, and 0%; red, 0%, 5%, 17%, 23%, and 0%; orange, 0%, 0%, 2%, 22%, and 72% of the total absorption area in A, B, C, D, and E, respectively. These intensities are the results of a global analysis of the entire set of Mössbauer spectra, including those for time-points not depicted. The weak feature at 0 mm/s most noticeable in B and C reflects a minor impurity in the samples. It accounts for only ~2% of the total Fe absorption, does not vary with the reaction time, and, therefore, cannot be associated with the peak at 1.5 mm/s.

implies that it is almost certainly a (μ-1,2-peroxo)diiron(III/III) complex similar to compound **P** in sMMO and the cognate complex in the *E. coli* R2-D84E variants (*16*, *19*, *21*, *22*, *30*).

Kinetics of the Mouse R2 Reaction by Stopped-Flow Absorption, Freeze-Quench EPR, and Freeze-Quench Mössbauer Spectroscopies. From time-dependent absorption spectra following the mixing of Fe(II)-complexed R2 with excess O_2 at 10 °C, the kinetics of the 700-nm absorption feature of the (μ-1,2-peroxo)diiron(III/III) complex (Figure 3; blue circles) and of the 416-nm feature of Y177• (Figure 3, purple circles) were obtained and are consistent with the hypothesis that the 700-nm-absorbing complex is on the pathway to the radical. The data suggest that the peroxide complex is not, however, the immediate precursor to Y177•;

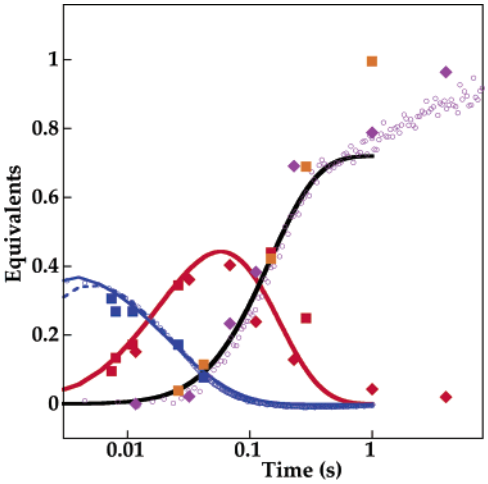

FIGURE 3: Kinetics of the (μ-1,2-peroxo)diiron(III/III) intermediate (blue symbols), **X** (red symbols), Y177• (purple symbols), and (μ-oxo)diiron(III/III) cluster (orange symbols) in the reaction of Fe(II)-complexed R2 at 10 °C with excess O_2. The open circles are data from a stopped-flow experiment that had concentrations after mixing of 0.15 mM R2, 0.6 mM Fe(II) (4 equiv), and 1.4 mM O_2. The filled squares are from the FQ Mösssbauer experiment described in the legend to Figure 2. The filled diamonds are from the FQ EPR experiment described in the legend to Figure 4. The raw stopped-flow data have been scaled to molar equivalents by assuming $\epsilon_{700} = 1500\ M^{-1}\ cm^{-1}$ for the (μ-1,2-peroxo)diiron(III/III) intermediate and $\epsilon_{416-(410+422)/2} = 235\ M^{-1}\ cm^{-1}$ for Y177• (*26*). The solid lines are simulations of the data according to Scheme 1 and the concentrations used in the FQ experiments. The dashed line is a simulation of the kinetics of the (μ-1,2-peroxo)diiron(III/III) complex with concentrations used in the SF experiments.

a regression analysis of the data from experiments with different reaction conditions yields rate constants for the decay of the 700-nm absorption feature that are always larger than the rate constants associated with the lag phase in the formation of Y177•, indicating the presence of at least one intervening reaction intermediate between the peroxide complex and Y177•. A previous mechanistic investigation on the O_2 reaction of mouse R2 (*26*) and the freeze-quench EPR and Mössbauer data presented below indicate that the intervening intermediate is the diiron(III/IV) cluster **X**.

In accord with a previous report (*26*), two well-resolved formation phases are detected for Y177• (Figure 3, purple circles). This observation was previously attributed to the presence of two forms of diiron sites in the Fe(II)-complexed R2 reactant. One form is ready to react with O_2 and gives the rapid phase of Y177• generation. The other form requires a rate-limiting Fe(II)-uptake step to convert to the O_2 reactive form and gives the slower formation phase (*26*). This hypothesis that R2 proteins preincubated with Fe(II) contain O_2-reactive and unreactive diiron sites and that conversion of the unreactive form to the O_2-reactive form occurs during the O_2 reaction by the uptake of Fe(II) was subsequently corroborated by a quantitative EPR investigation on metal binding by *E. coli* R2 (*31*). This study demonstrated that an anti-cooperative metal-binding effect exists between the two protomers within an R2 homodimer. The binding of Fe(II) in one protomer (i.e., the formation of O_2-reactive diiron(II/II) sites) was shown to prevent (or reduce) metal incorporation into the adjacent protomer (i.e., the retention of unoccupied metal binding sites). Furthermore, the binding of metal to the unoccupied metal binding sites was observed to occur during the O_2 reaction (*31*). These observations provide support for our earlier rationale for the two phases of Y177• formation.

The quantitative EPR study (*31*) also showed that the negative cooperativity in metal binding is removed or diminished by the presence of a high concentration of glycerol. Therefore, we investigated the effect of glycerol on the kinetics of the mouse R2 reaction. Indeed, the fraction of the total amplitude of Y177• formation in the fast phase was found to increase with increasing glycerol concentration up to 24% (w/w) (Figure S1 of the Supporting Information), consistent with the hypothesis that glycerol can alleviate anti-cooperativity in metal binding and thereby increase the fraction of fully occupied and O_2-reactive diiron sites in the protein reactant solution.[3] Even more significantly, the accumulation of the 700-nm feature of the (μ-1,2-peroxo)diiron(III/III) species increases proportionally (Figure S1, Supporting Information), providing further evidence that the complex is on the pathway to Y177•.

To define the reaction sequence and refine the spectroscopic characterization of the intermediates, a thorough kinetic analysis was carried out by FQ-EPR and FQ-Mössbauer methods. Consistent with our earlier conclusion that only two EPR detectable species, the diiron(III/IV) cluster **X** and Y177•, accumulate during the mouse R2 reaction (*26*), the EPR spectra of samples freeze-quenched during the reaction (Figure 4, A−C) can be reproduced (A′−C′) as linear combinations of the reference spectra of Y177• (spectrum D) and cluster **X** (spectrum E) (*10*). The concentrations of **X** and Y177• accumulated at each reaction time can be obtained from the relative contribution of each species determined through this reconstruction analysis and the total spin concentration determined from the double-integrated intensity of the spectrum. The resulting kinetic data are plotted in Figure 3 (diamonds). The kinetics of Y177• formation determined by EPR (Figure 3, purple diamonds) agree very well with those determined from the stopped-flow absorption experiments discussed above (Figure 3, purple circles). The formation and decay of **X** determined from EPR (Figure 3, red diamonds) are seen to occur between the decay of the 700-nm absorption feature of the peroxodiiron(III/III) complex (Figure 3, blue circles) and the formation of Y177• (Figure 3, purple symbols), indicating that **X** is indeed an intervening intermediate formed between the early forming peroxodiiron(III/III) complex and the final Y177• product.

As described in the previous section, the time-dependent Mössbauer spectra of samples freeze-quenched at various times after the mixing of Fe(II)-complexed R2 with O_2 (Figure 2) show the early formation of an Fe species that exhibits spectroscopic properties characteristic of a **P**-like (μ-1,2-peroxo)diiron(III/III) complex (Figure 2 spectrum B, blue line). As the peroxodiiron(III/III) complex decays, the paramagnetic spectrum of **X** (*11*, *26*) appears (Figure 2 spectrum C, red line). With time, this paramagnetic signature of **X** becomes more intense, reaching a maximum intensity at a reaction time close to 0.15 s (Figure 2 spectrum D, red line). At this reaction time, a pair of partially resolved quadrupole doublets (Figure 2 spectrum D, orange line)

[3] At even higher glycerol concentrations, the high viscosity of the reactant solutions and the resulting inefficient mixing become prohibitive.

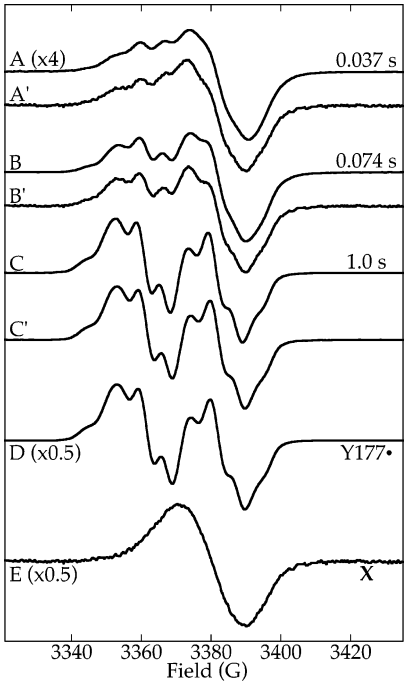

FIGURE 4: Component analysis of EPR spectra of samples obtained by mixing an O_2-free solution of 1.36 mM mouse R2 pre-complexed with 5.44 mM Fe(II) (4 equiv) in 100 mM Hepes (pH 7.6) and 24% glycerol with 2 equiv volumes of an O_2-saturated solution of the same buffer. In A−C, the first trace is the experimental spectrum of the sample freeze-quenched at the indicated reaction time, and the second trace (A′−C′) is the corresponding reconstruction by summation of the reference spectra for Y177• (spectrum D) and **X** (spectrum E). Spectrum D is of the 100-s sample. Spectrum E is of a sample obtained by equal-volume mixing at 10 °C of an O_2-free solution of 0.30 mM apo R2-Y177F and 1.2 mM Fe(II) with O_2-saturated buffer and freeze-quenching at a reaction time of 0.35 s. All spectra were recorded at 20 K with a microwave power of 6.3 μW and a modulation amplitude of 4 G. For A−D, a scan time of 160 s and a time constant of 0.16 s were used. For E, the scan time was increased to 1300 s and the time constant to 1.3 s. Integrated spectral intensities were related to concentration by use of a copper perchlorate standard, as previously described (*10*).

characteristic of the product (μ-oxo)diiron(III/III) cluster (*26*) have also become visible. At longer times, the signature of **X** decays, and the (μ-oxo)diiron(III/III)-associated doublets increase in intensity (data not shown). Eventually, at the completion of the reaction, the only recognizable feature in the Mössbauer spectrum is the signature of the (μ-oxo)diiron-(III/III) product (Figure 2 spectrum E, orange line). By decomposing these time-dependent spectra into their component features (those of reactant Fe(II) species, the (μ-1,2-peroxo)diiron(III/III) complex, **X**, and the (μ-oxo)diiron(III/III) product), the kinetics of each species were obtained. The results from the three independent methods agree well (Figure 3). Most importantly, the decay of the 700-nm absorption feature (Figure 3, blue circles) correlates with decay of the Mössbauer doublets associated with the (μ-1,2-peroxo)diiron(III/III) complex (Figure 3, blue squares). In this comparison, the use of a molar absorptivity of 1,500 M^{-1} cm^{-1} for the complex was found to give optimal agreement between the absorbance data and the molar equivalents of the complex determined by the area of the Mössbauer features. This value agrees well with those reported for the similar peroxide complexes (*18*, *20*, *32*). Also, the formation of the (μ-oxo)diiron(III/III) product determined from FQ-Mössbauer (Figure 3, orange squares) coincides with the formation of Y177• determined from absorption and FQ-EPR (Figure 3, purple circles and diamonds, respectively), providing evidence for the concomitant formation of the two constituents of the R2 cofactor. Consistent with the FQ-EPR results, the FQ-Mössbauer data also show that cluster **X** (Figure 3, red squares) is a transient intermediate that forms between the early (μ-1,2-peroxo)-diiron(III/III) complex and the final (μ-oxo)diiron(III/III)/Y177• product. The quantities of **X** determined by these two methods agree well for the formation phase but show scatter during the decay phase. This scatter is attributable to the large uncertainties involved in the quantification of **X** at longer reaction times, when its diminishing featureless EPR singlet spectrum is obscured by the developing sharply featured spectrum of Y177• and its magnetically split Mössbauer spectrum is obscured by overlapping features of a paramagnetic high-spin Fe(III) species that also develops late in the reaction. Nevertheless, the overall trend of the data is consistent with the hypothesis that **X** is a successor to the (μ-1,2-peroxo)diiron(III/III) complex and a precursor to Y177• and the (μ-oxo)diiron(III/III) cluster.

Mechanistic Subtleties Revealed by the Kinetic Data. If formation of the (μ-1,2-peroxo)diiron(III/III) complex from O_2 and Fe(II)-complexed R2 were to involve a single irreversible step, then its rapid formation (k_{obs} ~700 s^{-1} at this [O_2]) and much slower decay (k_{obs} ~60 s^{-1}) ought to lead to its accumulation to a concentration approaching ~0.8 of the initial concentration of the reactant complex and the final concentration of the products. In contrast, the maximal accumulation (~0.4 equiv) of the (μ-1,2-peroxo)diiron(III/III) intermediate determined by the Mössbauer and stopped-flow data is only approximately half the quantity of Y177• and the (μ-oxo)diiron(III/III) cluster (~0.8 equiv) produced in the fast phase of the reaction, indicating a more complex reaction mechanism.

The accumulation of the intermediate to a level that is insufficient to account for the quantities of the reaction products has several possible explanations. First, the intermediate might not be on the pathway to the products but, rather, on a parallel, unproductive pathway. This possibility, however, is not supported by the spectroscopic and kinetic data (Figures 2−4). The data show that as the (μ-1,2-peroxo)-diiron(III/III) complex decays, the only detectable Fe species that forms in an amount sufficient to account for the loss of the peroxide is **X**, unambiguously indicating that **X** is a successor to the (μ-1,2-peroxo)diiron(III/III) complex. Because **X** has been established as the precursor to the tyrosyl radical/(μ-oxo)diiron(III/III) cofactor in R2 (*8*−*10*), it follows then that the rapidly forming (μ-1,2-peroxo)diiron(III/III) complex is on the productive pathway. Furthermore, although the rate constant for the decay of **X** is also an order of magnitude less than its formation rate constant, the maximal accumulation of **X** (~0.44 equiv) is comparable to that of the (μ-1,2-peroxo)diiron(III/III) complex and is also only about half the amount of its decay product, the (μ-oxo)diiron-(III/III) cluster, produced in the fast phase. This latter observation provides further evidence for the association between the (μ-1,2-peroxo)diiron(III/III) complex and **X** and demands an explanation other than that the peroxide complex is off-pathway.

An alternative explanation is that the formation of the (μ-1,2-peroxo)diiron(III/III) complex is reversible. Competition

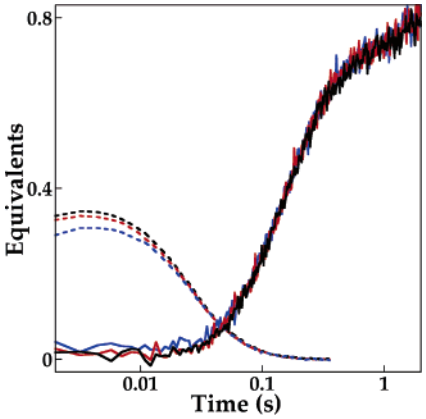

FIGURE 5: Dependence on O_2 concentration of the kinetics of formation and decay of the (μ-1,2-peroxo)diiron(III/III) intermediate and formation of Y177• in the reaction of Fe(II)-complexed R2 with excess O_2 at 10 °C. The stopped-flow traces for A_{700} (dashed) and $A_{416} - (A_{410} + A_{422})/2$ (solid) were scaled to molar equivalents by using the estimated molar absorptivities given in the legend to Figure 3. All three reactions depicted had R2 and Fe(II) concentrations of 0.15 mM and 0.6 mM, respectively, after mixing. The estimated O_2 concentrations were 0.95 mM (black), 0.71 mM (red), and 0.48 mM (blue). All reactions contained 24% glycerol.

from the reverse reaction would diminish its accumulation. This possibility was evaluated by the variation of reactant concentrations in stopped-flow experiments (Figure 5). For reversible formation, the suppression of accumulation would be mitigated by increasing reactant concentration such that the quantity to accumulate would show an approximately hyperbolic dependence on the concentration of the (pseudo-first-order) excess reactant. In contrast, the kinetics of the absorbance at 700 nm and its maximum value are seen in Figure 5 to depend only to a minor extent on [O_2]. Although the range of [O_2] interrogated is insufficient to permit the determination of the rate constant for the reverse reaction, the observed lack of concentration dependence does rule out reversibility as the primary explanation for the diminished accumulation of the (μ-1,2-peroxo)diiron(III/III) complex.

A third possible explanation for the less-than-expected accumulation of the (μ-1,2-peroxo)diiron(III/III) complex is the rapid and reversible conversion of the complex to a second intermediate state. This rapid interconversion would cause the peroxide complex and the Fe intermediate to which it converts to be kinetically linked. In other words, they would grow in and decay together as a single entity. The Mössbauer data were scrutinized for evidence of the formation and decay of an additional Fe complex in parallel with the (μ-1,2-peroxo)diiron(III/III) complex, but no such Fe intermediate could be detected (see, for example, Figure 2).

With these possibilities eliminated, a slightly more complex scheme for the mouse R2 reaction was considered (Scheme 1). As demonstrated in previous studies (*26*, *31*) and discussed above, the observed fast and slow formation phases of Y177• indicate heterogeneity in the Fe(II)-complexed R2, which contains fully occupied, possibly partially occupied, and unoccupied diiron sites. Whereas the diiron(II/II) sites are ready to react with O_2, the unoccupied and partially occupied diiron sites require a slow (<0.5 s^{-1} (*26*)) Fe-uptake step before they can react with O_2. In the present study, the less-than-expected accumulation of the (μ-1,2-peroxo)diiron(III/III) intermediate indicates further that heterogeneity in O_2 reactivity must be present even among the fully occupied diiron(II/II) sites. The data can be explained if it is assumed that a fraction (60%) of the diiron(II/II) clusters (form B in Scheme 1) reacts rapidly with O_2 while a second, somewhat smaller fraction (40%) of the diiron(II/II) clusters (form C in Scheme 1) must first convert to the reactive form with a rate constant comparable to that for the decay of the (μ-1,2-peroxo)diiron(III/III) intermediate. Then, the accumulation of the peroxide intermediate from this latter fraction of the diiron(II/II) clusters would be suppressed because of effective competition from the decay of the intermediate. With this assumption, the kinetic data can be simulated. The results are shown in Figure 3 (solid lines). The proposed heterogeneity for the diiron(II/II) clusters could be due to an anti-cooperative allosteric effect, similar to that detected for metal incorporation into apo-R2 (*26*, *31*), also for O_2 activation. That is, the reaction of O_2 with the diiron(II/II) site in one protomer may induce a

Scheme 1: Scheme Used in the Simulation of the Kinetic Data from the Reaction of Fe(II)-Complexed R2 with O_2 at 10 °C

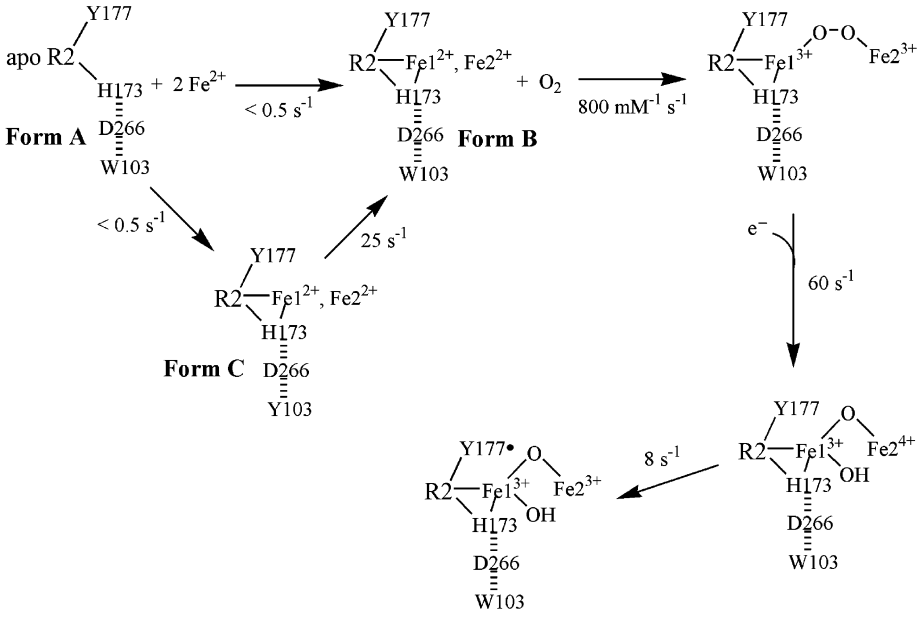

protein conformational change that inhibits the diiron(II/II) site of the neighboring protomer from reacting with O_2. If the Fe(II)-complexed R2 contains a significant fraction of fully complexed Fe(II)-R2 (a reasonable assumption given the Fe/R2 ratio of ~4 and the presence of 24% glycerol, which the quantitative EPR study showed diminishes anti-cooperativity in metal binding), then this anti-cooperative O_2-reactivity effect would prevent a significant fraction of the diiron(II/II) sites from reacting immediately with O_2, resulting in the slow phase.

In conclusion, the stopped-flow absorption, FQ-Mössbauer, and FQ-EPR data have demonstrated the rapid accumulation of a precursor to cluster **X** in the reaction of wild-type mouse R2 with O_2. The complex displays spectroscopic properties similar to those of the (μ-1,2-peroxo)diiron(III/III) intermediates detected in the reactions of sMMO (*12*, *13*) and D84E variants of *E. coli* R2 (*16*, *18*−*21*), providing evidence for the unifying hypothesis that O_2 activation by different diiron-carboxylate proteins commences with a common diiron-O_2 adduct, namely, the (μ-1,2-peroxo)diiron(III/III) complex. This finding provides important experimental validation of recent computational studies (e.g., ref 16 (*16*)) interrogating possible pathways and points of divergence in O_2 activation by the diiron proteins because these studies have generally proposed a common complex of this structural type as an intermediate. Prior to this work, evidence had been obtained for the accumulation of such a complex in the reaction of wild-type *E. coli* R2 (*17*), but the modest accumulation and very rapid decay of the complex in that case made it difficult to define its kinetics. In comparison with the complex detected in *E. coli* R2, the somewhat faster formation and significantly slower decay of the complex in mouse R2 lead to greater accumulation and provide just enough of a technical advantage to permit its kinetics to be studied here. Interestingly, the kinetic data reveal surprising mechanistic complexity that is probably related to influences of protein conformational dynamics on both Fe(II) binding and diiron-(II/II) cluster O_2 reactivity. The minimal mechanistic scheme that can accommodate the kinetic data requires the assumption of two forms of diiron(II/II) clusters with distinct O_2 reactivity. We have interpreted this apparent heterogeneity in the diiron(II/II) clusters as the result of an anti-cooperative allosteric effect between the two protomers within the homodimeric R2 protein. The physiological significance of this hypothetical allosteric effect is currently not known. However, mechanistic investigations of other diiron-carboxylate enzymes, for example, the soluble stearoyl-acyl carrier protein Δ^9 desaturase (*33*, *34*), suggest that such conformational effects on O_2 reactivity are not unique to R2.

SUPPORTING INFORMATION AVAILABLE

Figure showing the effect of glycerol concentration and temperature on the kinetics of formation and decay of the (μ-1,2-peroxo)diiron(III/III) intermediate and the formation of Y177• monitored by stopped-flow absorption. This material is available free of charge via the Internet at http://pubs.acs.org.

REFERENCES

1. Nordlund, P., and Eklund, H. (1995) Di-iron-carboxylate proteins, *Curr. Opin. Struct. Biol. 5*, 758−766.
2. Wallar, B. J., and Lipscomb, J. D. (1996) Dioxygen activation by enzymes containing binuclear non-heme iron clusters, *Chem. Rev. 96*, 2625−2657.
3. Solomon, E. I., Brunold, T. C., Davis, M. I., Kemsley, J. N., Lee, S.-K., Lehnert, N., Neese, F., Skulan, A. J., Yang, Y.-S., and Zhou, J. (2000) Geometric and electronic structure/function correlations in non-heme iron enzymes, *Chem. Rev. 100*, 235−349.
4. Tshuva, E. Y., and Lippard, S. J. (2004) Synthetic models for non-heme carboxylate-bridged diiron metalloproteins: strategies and tactics, *Chem. Rev. 104*, 987−1012.
5. Atkin, C. L., Thelander, L., and Reichard, P. (1973) Iron and free radical in ribonucleotide reductase. Exchange of iron and Mössbauer spectroscopy of the protein B2 subunit of the *Escherichia coli* enzyme, *J. Biol. Chem. 248*, 7464−7472.
6. Sjöberg, B.-M., Reichard, P., Gräslund, A., and Ehrenberg, A. (1977) Nature of the free radical in ribonucleotide reductase from *Escherichia coli*, *J. Biol. Chem. 252*, 536−541.
7. Larsson, A., and Sjöberg, B.-M. (1986) Identification of the stable free radical tyrosine residue in ribonucleotide reductase, *EMBO J. 5*, 2037−2040.
8. Bollinger, J. M., Jr., Edmondson, D. E., Huynh, B. H., Filley, J., Norton, J. R., and Stubbe, J. (1991) Mechanism of assembly of the tyrosyl radical-dinuclear iron cluster cofactor of ribonucleotide reductase, *Science 253*, 292−298.
9. Bollinger, J. M., Jr., Stubbe, J., Huynh, B. H., and Edmondson, D. E. (1991) Novel diferric radical intermediate responsible for tyrosyl radical formation in assembly of the cofactor of ribonucleotide reductase, *J. Am. Chem. Soc. 113*, 6289−6291.
10. Bollinger, J. M., Jr., Tong, W. H., Ravi, N., Huynh, B. H., Edmondson, D. E., and Stubbe, J. (1994) Mechanism of assembly of the tyrosyl-diiron(III) cofactor of *E. coli* ribonucleotide reductase. 2. Kinetics of the excess Fe^{2+} reaction by optical, EPR, and Mössbauer spectroscopies, *J. Am. Chem. Soc. 116*, 8015−8023.
11. Sturgeon, B. E., Burdi, D., Chen, S., Huynh, B. H., Edmondson, D. E., Stubbe, J., and Hoffman, B. M. (1996) Reconsideration of **X**, the diiron intermediate formed during cofactor assembly in *E. coli* ribonucleotide reductase, *J. Am. Chem. Soc. 118*, 7551−7557.
12. Lee, S., Nesheim, J., and Lipscomb, J. (1993) Transient intermediates of the methane monooxygenase catalytic cycle, *J. Biol. Chem. 268*, 21569−21577.
13. Liu, K. E., Wang, D., Huynh, B. H., Edmondson, D. E., Salifoglou, A., and Lippard, S. J. (1994) Spectroscopic detection of intermediates in the reaction of dioxygen with the reduced methane monooxygenase/hydroxylase from *Methylococcus capsulatus* (Bath), *J. Am. Chem. Soc. 116*, 7465−7466.
14. Baldwin, J., Krebs, C., Ley, B. A., Edmondson, D. E., Huynh, B. H., and Bollinger, J. M., Jr. (2000) Mechanism of rapid electron transfer during oxygen activation in the R2 subunit of *Escherichia coli* ribonucleotide reductase. 1. Evidence for a transient tryptophan radical, *J. Am. Chem. Soc. 122*, 12195−12206.
15. Edmondson, D. E., and Huynh, B. H. (1996) Diiron-cluster intermediates in biological oxygen activation reactions, *Inorg. Chim. Acta 252*, 399−404.
16. Skulan, A. J., Brunold, T. C., Baldwin, J., Saleh, L., Bollinger, J. M., Jr., and Solomon, E. I. (2004) Nature of the peroxo intermediate of the W48F/D84E ribonucleotide reductase variant: Implications for O_2 activation by binuclear non-heme iron enzymes, *J. Am. Chem. Soc. 126*, 8842−8855.
17. Tong, W. H., Chen, S., Lloyd, S. G., Edmondson, D. E., Huynh, B. H., and Stubbe, J. (1996) Mechanism of assembly of the diferric cluster-tyrosyl radical cofactor of *Escherichia coli* ribonucleotide reductase from the diferrous form of the R2 subunit, *J. Am. Chem. Soc. 118*, 2107−2108.
18. Bollinger, J. M., Jr., Krebs, C., Vicol, A., Chen, S., Ley, B. A., Edmondson, D. E., and Huynh, B. H. (1998) Engineering the diiron site of *Escherichia coli* ribonucleotide reductase protein R2 to accumulate an intermediate similar to $\mathbf{H}_{peroxo}$, the putative peroxodiiron(III) complex from the methane monooxygenase catalytic cycle, *J. Am. Chem. Soc. 120*, 1094−1095.
19. Moënne-Loccoz, P., Baldwin, J., Ley, B. A., Loehr, T. M., and Bollinger, J. M., Jr. (1998) O_2 activation by non-heme diiron proteins: Identification of a symmetric μ-1,2-peroxide in a mutant of ribonucleotide reductase, *Biochemistry 37*, 14659−14663.
20. Baldwin, J., Voegtli, W. C., Khidekel, N., Moënne-Loccoz, P., Krebs, C., Pereira, A. S., Ley, B. A., Huynh, B. H., Loehr, T. M., Riggs-Gelasco, P. J., Rosenzweig, A. C., and Bollinger, J. M., Jr. (2001) Rational reprogramming of the R2 subunit of *Escherichia*

coli ribonucleotide reductase into a self-hydroxylating monooxygenase, *J. Am. Chem. Soc. 123*, 7017−7030.

21. Baldwin, J., Krebs, C., Saleh, L., Stelling, M., Huynh, B. H., Bollinger, J. M., Jr., and Riggs-Gelasco, P. (2003) Structural characterization of the peroxodiiron(III) intermediate generated during oxygen activation by the W48A/D84E variant of ribonucleotide reductase protein R2 from *Escherichia coli*, *Biochemistry 42*, 13269−13279.
22. Voegtli, W. C., Khidekel, N., Baldwin, J., Ley, B. A., Bollinger, J. M., Jr., and Rosenzweig, A. C. (2000) Crystal structure of the ribonucleotide reductase R2 mutant that accumulates a μ-1,2-peroxodiiron(III) intermediate during oxygen activation, *J. Am. Chem. Soc. 122*, 3255−3261.
23. Saleh, L., Kelch, B. A., Pathickal, B. A., Baldwin, J., Ley, B. A., and Bollinger, J. M., Jr. (2004) Mediation by indole analogues of electron transfer during oxygen activation in variants of *Escherichia coli* ribonucleotide reductase R2 lacking the electron-shuttling tryptophan 48, *Biochemistry 43*, 5943−5952.
24. Saleh, L., Krebs, C., Ley, B. A., Naik, S., Huynh, B. H., and Bollinger, J. M., Jr. (2004) Use of a chemical trigger for electron transfer to characterize a precursor to cluster **X** in assembly of the iron-radical cofactor of *Escherichia coli* ribonucleotide reductase, *Biochemistry 43*, 5953−5964.
25. Krebs, C., Chen, S., Baldwin, J., Ley, B. A., Patel, U., Edmondson, D. E., Huynh, B. H., and Bollinger, J. M., Jr. (2000) Mechanism of rapid electron transfer during oxygen activation in the R2 subunit of *Escherichia coli* ribonucleotide reductase. 2. Evidence for and consequences of blocked electron transfer in the W48F variant, *J. Am. Chem. Soc. 122*, 12207−12219.
26. Yun, D., Krebs, C., Gupta, G. P., Iwig, D. F., Huynh, B. H., and Bollinger, J. M., Jr. (2002) Facile electron transfer during formation of cluster **X** and kinetic competence of **X** for tyrosyl radical production in protein R2 of ribonucleotide reductase from mouse, *Biochemistry 41*, 981−990.
27. Bollinger, J. M., Jr., Tong, W. H., Ravi, N., Huynh, B. H., Edmondson, D. E., and Stubbe, J. (1995) Use of rapid kinetics methods to study the assembly of the diferric-tyrosyl radical cofactor of *E. coli* ribonucleotide reductase, *Methods Enzymol. 258*, 278−303.
28. Ravi, N., Bollinger, J. M., Jr., Huynh, B. H., Edmondson, D. E., and Stubbe, J. (1994) Mechanism of assembly of the tyrosyl radical-diiron(III) cofactor of *E. coli* ribonucleotide reductase: 1. Mössbauer characterization of the diferric radical precursor, *J. Am. Chem. Soc. 116*, 8007−8014.
29. Parkin, S. E., Chen, S., Ley, B. A., Mangravite, L., Edmondson, D. E., Huynh, B. H., and Bollinger, J. M., Jr. (1998) Electron injection through a specific pathway determines the outcome of oxygen activation at the diiron cluster in the F208Y mutant of *Escherichia coli* ribonucleotide reductase protein R2, *Biochemistry 37*, 1124−1130.
30. Voegtli, W. C., Sommerhalter, M., Saleh, L., Baldwin, J., Bollinger, J. M., Jr., and Rosenzweig, A. C. (2003) Variable coordination geometries at the diiron(II) active site of ribonucleotide reductase R2, *J. Am. Chem. Soc. 125*, 15822−15830.
31. Pierce, B. S., Elgren, T. E., and Hendrich, M. P. (2003) Mechanistic implications for the formation of the diiron cluster in ribonucleotide reductase by quantitative EPR spectroscopy, *J. Am. Chem. Soc. 125*, 8748−8759.
32. Valentine, A. M., Stahl, S. S., and Lippard, S. J. (1999) Mechanistic studies of the reaction of reduced methane monooxygenase hydroxylase with dioxygen and substrates, *J. Am. Chem. Soc. 121*, 3876−3887.
33. Lyle, K. S., Haas, J. A., and Fox, B. G. (2003) Rapid-mix and chemical quench studies of ferredoxin-reduced stearoyl-acyl carrier protein desaturase, *Biochemistry 42*, 5857−5866.
34. Fox, B. G., Lyle, K. S., and Rogge, C. E. (2004) Reactions of the diiron enzyme stearoyl-acyl carrier protein desaturase, *Acc. Chem. Res. 37*, 421−429.

BI061717N